ILC-HiGrade-Report-2012-002-1

Statistical analysis of quench locations of 1.3 GHz superconducting rf cavities at DESY

F. Schlander*

October 5, 2012

Abstract

A statistical analysis of quench locations in superconducting rf cavities based on a sample of 31 cavity tests is presented. The quenches were located using the second sound technique and were carried out from April 2010 to May 2012. The sample comprises cavities from several recent production series and includes the reference cavities produced for the European XFEL.

*DESY, Hamburg, Germany

1 Introduction

The origin of thermal quenches in superconducting rf (SRF) cavities can be related to various causes that depend on the field strength. While at low field impurities on the material surface are often readily recognized and by now have mostly been eliminated by appropriate steps in the cavity manufacturing process the origin of quenches at high fields is more subtle and less straightforward to assess. The assembly of individual cells to 9-cell cavities that are typically used for large scale applications introduces extra handling steps that may affect the surface properties.
The measurement of thermal breakdown is still an involved process and require explicit mounting of resistor chains or grids on the outer surface of a cavity. The prediction of quench locations based on identified surface irregularities from an optical inspection [1] has shown some success [2, 3]. This analysis uses a different approach. A sample of 31 recent cavities could be investigated including the second sound technique for quench location. The method is about 10 times faster than resistive temperature mapping and dramatically eases assembly of the setup. This dataset is introduced in the next section. The analysis investigates the locations of quenches in a statistical fashion and distinguished longitudinal and azimuthal coordinates.

2 Data sample

The analysis of quenches located by second sound [4] is based on a sample of 31 cavity tests. In most cases all passband modes of the cavity were excited so that up to nine different quench locations per cavity could be measured. Typically four to five spots were found. Depending on the passband mode the configuration of cells exposed to the peak field varies. These cells are hence more like to quench. The resulting bias in the distribution has to be corrected for. Some cavities are not quench-limited in all modes (or the quench location could not be reconstructed). The standard π-mode exposes all cells to the same field; 26 quench locations were so identified. For all other modes ($8/9\pi$ to $1/9\pi$-mode) 18 to 22 quench locations have been measured. The analysis takes into account the cells exposed to the highest field (up to 4 maximum) and otherwise assumes an equal probability for quench in each of these cells.
Figure 1 shows the coordinate system [5] used for the cavities of the European XFEL, which is also used in this analysis.
The data sample includes all quenches from pure thermal breakdown (BD) and those quenches that occur in conjunction with radiation, where the threshold has been placed at 10^{-2} mGy/min. The later quenches are referred to as BD_FE. An overview of the observed quench locations is shown in Fig. 2. For ease of reading, the z-coordinate has been replaced by cell numbers and the horizontal grid marks the equator positions. The coordinates are transformed as $z = 115.4 \times (x - 1)\,\mathrm{mm}$, while x is the cell number.
The observed distribution is not uniform. The region from $270° \geq \Phi \geq 90°$ registers more quenches than the center of the plot. In addition the *outer* cells (1-2 and 8-9) also suffer more often from quench than the inner cells. The large number of quenches

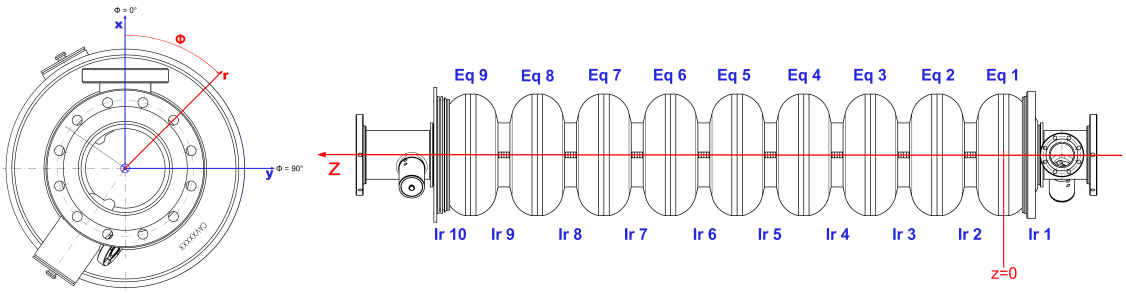

(a) angular coordinate Φ (b) beam axis coordinate z

Figure 1: The coordinate system of the 1.3 GHz SRF cavities, which is used for the following discussion.

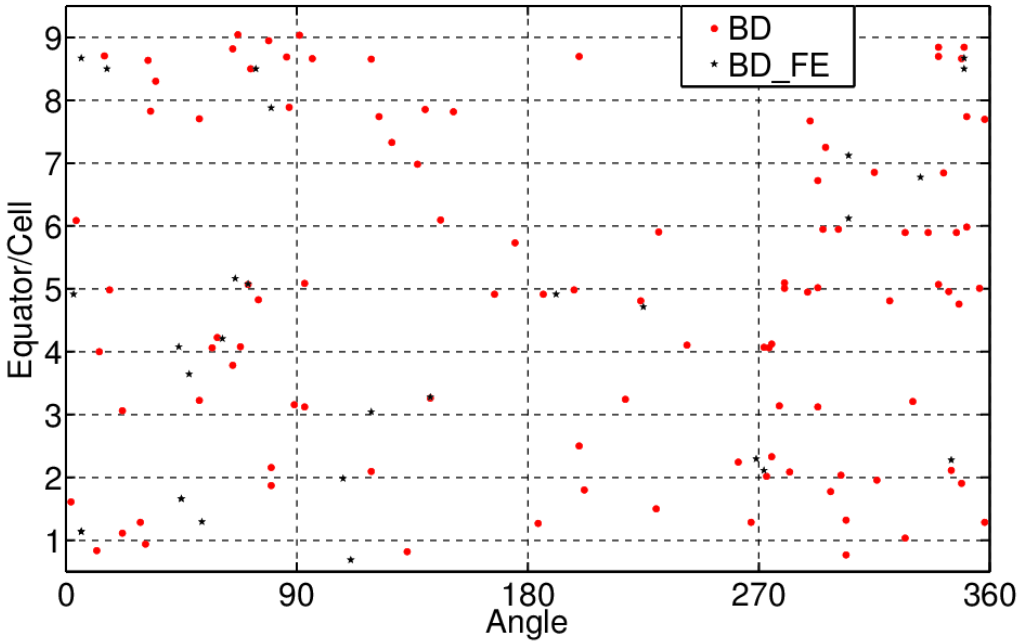

Figure 2: Scatter plot of all 189 quench locations measured by second sound at DESY. The angle is given as described in Fig. 1. The two breakdown situations are distinguished: BD without and BD_FE with significant field emission.

observed in cell 5 is expected easily, since this cell is exposed to the highest field in five out of the nine passband modes.

3 Quench distribution along the cavity axis

The total number N of quenches sums up to 189 and contains all events of thermal breakdown including the cases with excessive field emission. Assuming naively a uniform

distribution in the cavity results in 21 quenches as the expectation for the number of quenches in each cell. The thermal breakdown will occur preferentially in one of the cells containing the maximum rf field as has been confirmed e.g. in [2]. Correspondingly the number of modes generating the maximum field in each cell have to be considered as well: for cells 2 and 8, there are 2 passband modes where the rf field reaches the maximum amplitude, cell number 5 is exposed to the maximum rf field in all odd $\frac{n}{9}\pi$ passband modes. All other cells experience 3 modes with peak field. Hence a total of 27 cells (configurations) with highest fields can be distinguished; on average there are three quench possibilities per cell.
As a consequence the expected number $E(x)$ of quenches for each cell x is calculated as follows:

$$E(x) = \frac{\text{modes with maximum field in cell}(x)}{27} \times N. \tag{1}$$

Note that no uncertainty is attributed to the number N, which is simply taken as the expectation value for the number of quenches for this sample. The following study will reveal whether this assumption is supported by the data.
The observed number of quenches per cell is shown in Fig. 3, including the expected value $E(x)$ marked by a dashed line. In the absence of further information on each cavity and cell all measurements are treated independently. The uncertainties given in the plots in this section are the statistical standard deviation of a binomial distribution.

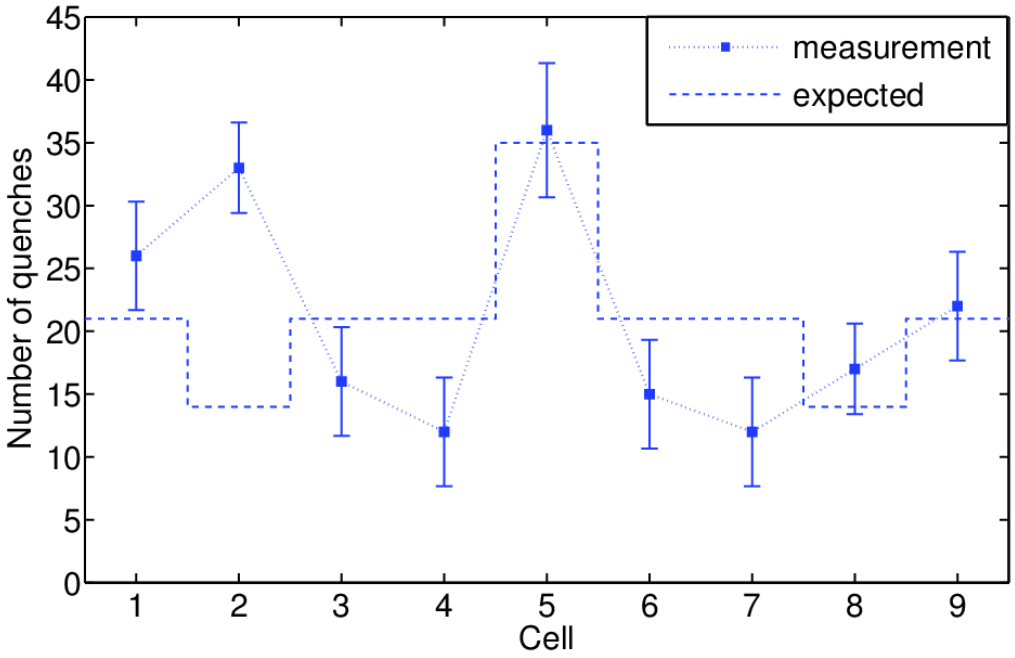

Figure 3: The total number of quenches observed in each cell. The dashed line shows the expected number of quenches, which accounts for the varying number of cells with maximum rf field in the nine passband modes.

It is obvious that there is a large difference between the expected number of quenches and the measured frequency in cell 2. While there may be a few false attributions to cell 2 due to field emission confused at the irises between cells 1-2 or 2-3 this number is sufficiently small not to affect the basic observation.
One may speculate about the origin: surface contamination by dust, humidity or gas residuals, since the flange at this end of the cavity is the last one mounted inside the cleanroom? The cavity is pumped and vented from this side and the connection to the pumping system is done in a separate cleanroom. The chance of such a contamination is low due to the handling experience gained in the cavity treatment and assembly at DESY [6].
So can the difference be traced to the specific details of the cavity manufacture and in particular manufacturer? This correlation is explored in Fig. 4 which differentiates the distribution of Fig. 3 by vendor engaged in providing cavities to DESY. While the number of counts for cells 3 to 9 are within the expected range or even less, for cell 2 an excess is seen for both vendors. Cell 1 shows a distinctly different behaviour: while for vendor A the number of counts are in the expected range vendor B exhibits a number of quenches 4σ beyond expectation. Within the limited statistics there are strong indications that differing production processes at the vendors cause this difference in the distribution, especially for end-cell 1.
Assuming constant probability $p(x)$ for a quench to occur in cell x at a given field the distribution of Fig. 4 can be cast into a probability which are shown in Fig. 5.
Here the probability $P(n \geq k)$ that the number n reaches or exceeds the number k of observed quenches in the sample is shown. In analogy to (1) the individual probability is defined as

$$p(x) = \frac{\text{modes with maximum field in cell}(x)}{27} \tag{2}$$

and hence

$$P(n \geq k) = \sum_{k}^{n} \binom{n}{k} p^k (1-p)^{n-k}. \tag{3}$$

The observation in Fig. 5 shows that the number of quenches occuring in cell 2 are very unlikely with $P \approx 10^{-3}$, while for cell 1 it varies by vendor: for vendor A the probability is $P \approx 0.86$, but for vendor B it is $P \approx 7 \times 10^{-3}$, as already has been shown in Fig. 4.

3.1 Thermal breakdown fields in each cell

For further investigation and not to bias distributions from now on quench locations occuring in multiple modes have been excluded out by allowing no additional quenches within a limit of $\Delta z = \pm 20\,\text{mm}$ and $\Delta\Phi = \pm 10^\circ$ around a previous quench location. This results in 103 events to be included in this analysis.
As about 25% of the non-BCP [7] treated cells quench below 30 MV/m, the distribution of these quenches by cell is of interest. Fig. 6 shows the integrated number of quenches in relation to the quench field for each cell. As has been shown in Fig. 3, a large excess of quenches is seen in cells 1 and 2. Comparison with the quench fields show that eight out of 15 quenches in cell 2 occur at fields below 20 MV/m. A check of the underlying data

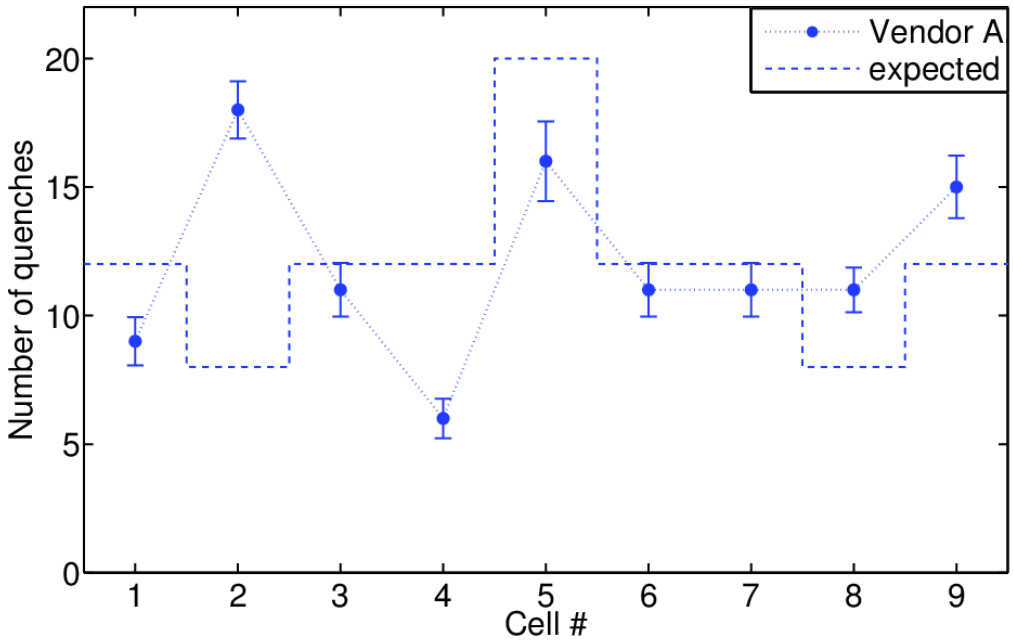

(a) Vendor A

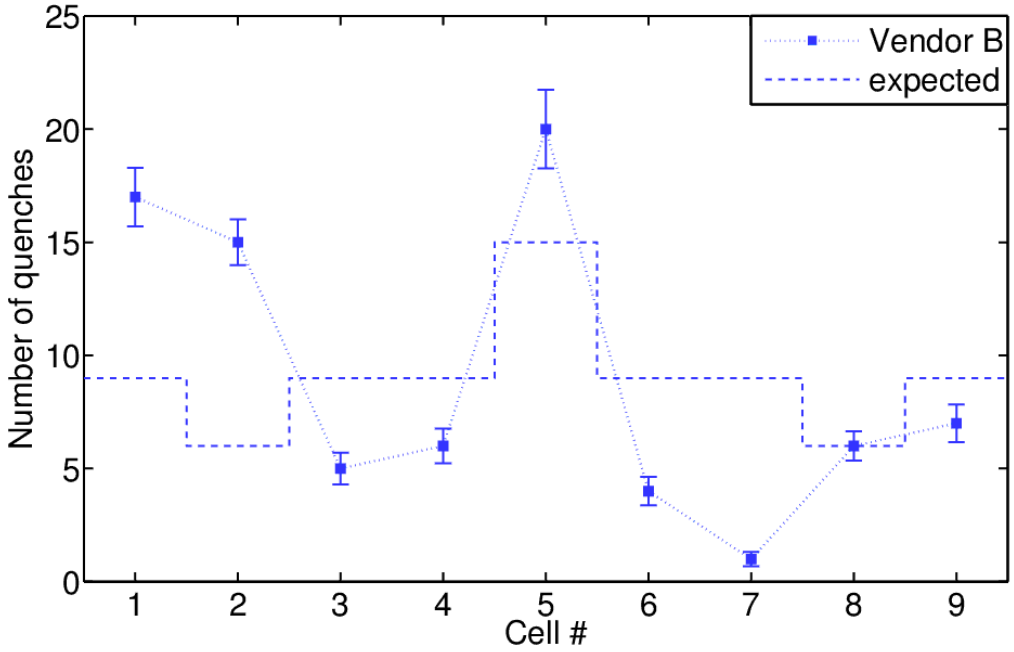

(b) Vendor B

Figure 4: Observation of quenches per cell, separated for each vendor. The dashed line shows the expected number for each cell.

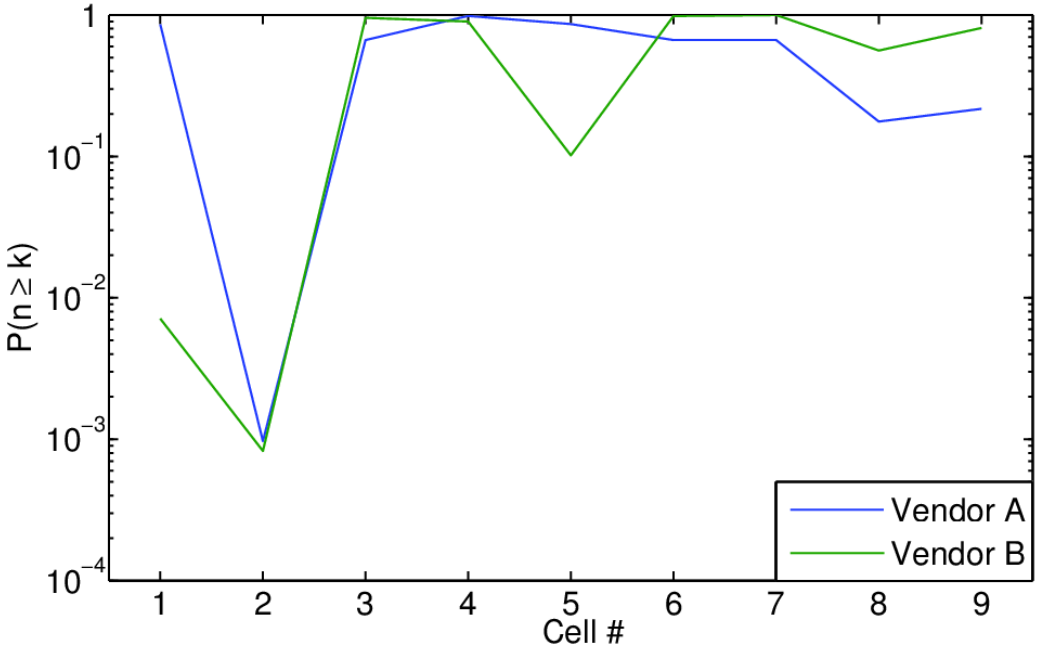

Figure 5: The probabilities for the quench distribution as shown in Fig. 4.

indicates that cavity AC127 test 8 shows field emission below the BD_FE threshold in $4/9\pi$-$1/9\pi$, and hence populate three different locations in cell 2, which are most likely the same position in modes $4/9\pi$ to $2/9\pi$. In addition, one of the quench locations with low field (CAV00506 test 2) has been detected close to iris 2 and cannot be properly assigned to cell 1 or 2. A few quenches below this threshold are also seen in cell 1. The quenches at 0 MV/m are errors, which can appear if the quench occurs close to the iris region and hence a proper assignment to a cell is not possible within uncertainty. Cells 4 to 9 experience almost all quenches beyond 30 MV/m and show a strong increase from 30 to 40 MV/m. It seems that the suspicious cells 1 and 2 with an excess of quenches compared to the expectation perform weakest at low fields while all other cells show a more uniform behaviour: the quenches increase as the fields is raised beyond 30 MV/m.

4 Angular distribution

Fig. 7 shows the angular distribution of all quench locations, also including BD_FE limited modes, in bins of 45° but excluding multiple quenches nearby. Again this results in 121 quench locations. An uniform distribution is expected, since the magnetic field amplitudes azimuthally along the cavity surface are rotationally symmetric. The angular region between 270° and 90° shows more quenches than the statistical average value of about 15 per bin while on the opposite side much less quenches are observed. Again, the uncertainties are those of a binomial distribution, for reasons explained earlier. The distribution initiated an investigation of dependencies of the quench locations

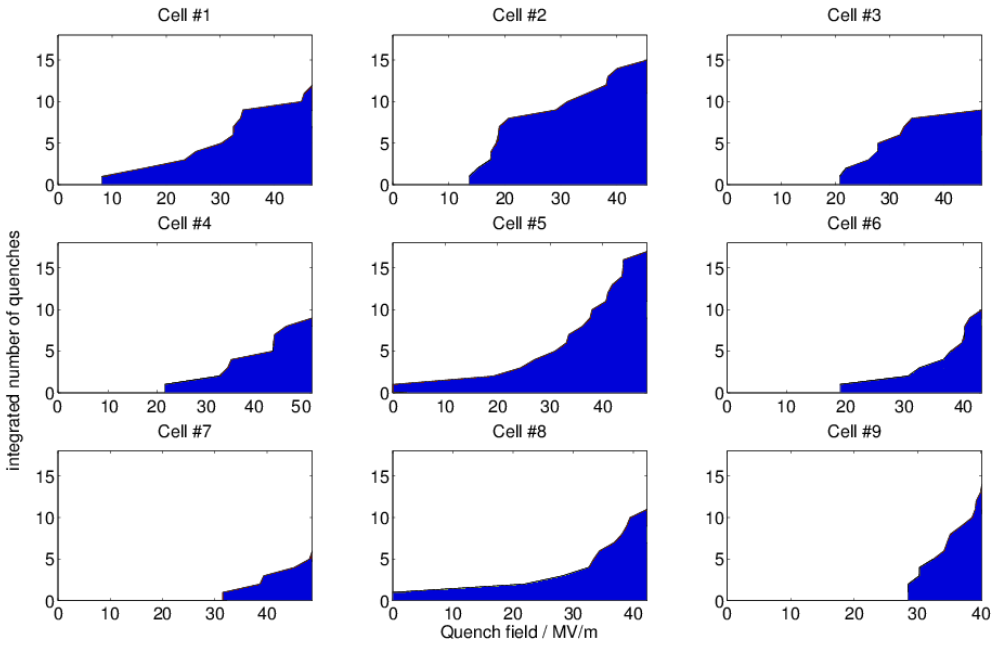

Figure 6: The integrated number of quenches corresponding to the field achieved in each quenching cell. Cell 2 showed more quenches than expected (cf. Fig. 3) also shows most of the quench onsets below 30 MV/m compared to all other cells.

with preparation and assembly steps.

4.1 Systematic contributions

It is important to verify that the second sound measurement technique itself does not introduce a bias. Such biases could be due to varying sensitivity or broken OSTs. About ten cavity tests have been carried out with quench detection using second sound and temperature mapping simultaneously. Although these tests have shown consistent results, all tests carried out with temperature mapping [8] up to three years before the installation of the second sound system have been examined: The quench locations found by the T-map system are given in Fig. 8 and show, although with lower statistics (nine tests with defined quench locations), a similar angular distribution.
To exclude systematic uncertainties along the z-axis, the data available is not sufficient.

4.1.1 Vendor dependent effects

For exclusion of vendor dependent effects, Fig. 9 shows the angular distribution of quench locations for both vendors providing cavities at DESY separately. In contrast to the longitudinal distribution discussed in the previous section, there is no obvious indication for one vendor with a significant concentration of quenches in a certain angular range.

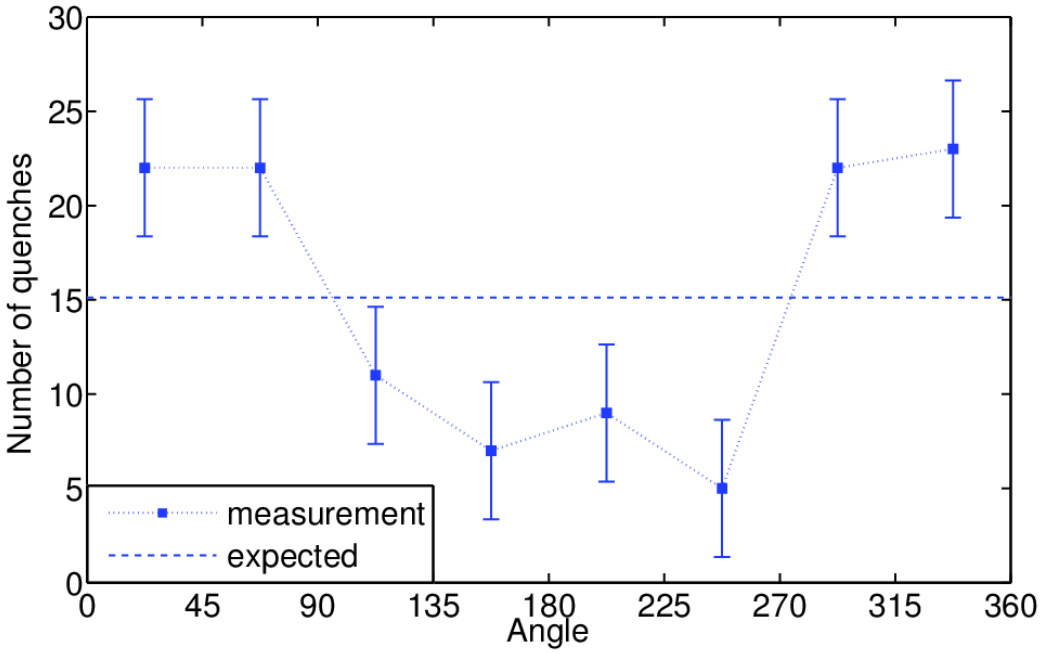

Figure 7: Angular quench distribution after filtering for multiple quenches.

Both diagrams show an excess of quench locations in the previously discussed range around the power coupler flange, while vendor A exceeds expectation at $\Phi > 270°$ and vendor B at $\Phi < 90°$. There must be other mechanisms at work, or both vendors apply the same production step causing this distinctive feature.

4.1.2 Horizontal cavity preparation steps

Another possible source of the angular clustering might be found in the preparation steps of the cavities. If preparation steps take place horizontally and with a preferred angular orientation - the power coupler flange pointing downwards, they could influence the angular distribution of quench spots. This leads to the hypothesis that any kind of particles, humidity or other contamination on the surface accumulates in the lower half, i.e. in the angular region of the power coupler.
The 800 °C baking for reducing the hydrogen contamination is done in a horizontal furnace, but as the cavity is placed in the furnace with an arbitrary angle, the baking can be excluded as a cause of the observed distribution.
Further preparation steps proceeding in the cleanroom including electropolishing, cavity handling and mounting of the flanges do not have a preferred angular orientation either and can be ruled out as well [6].

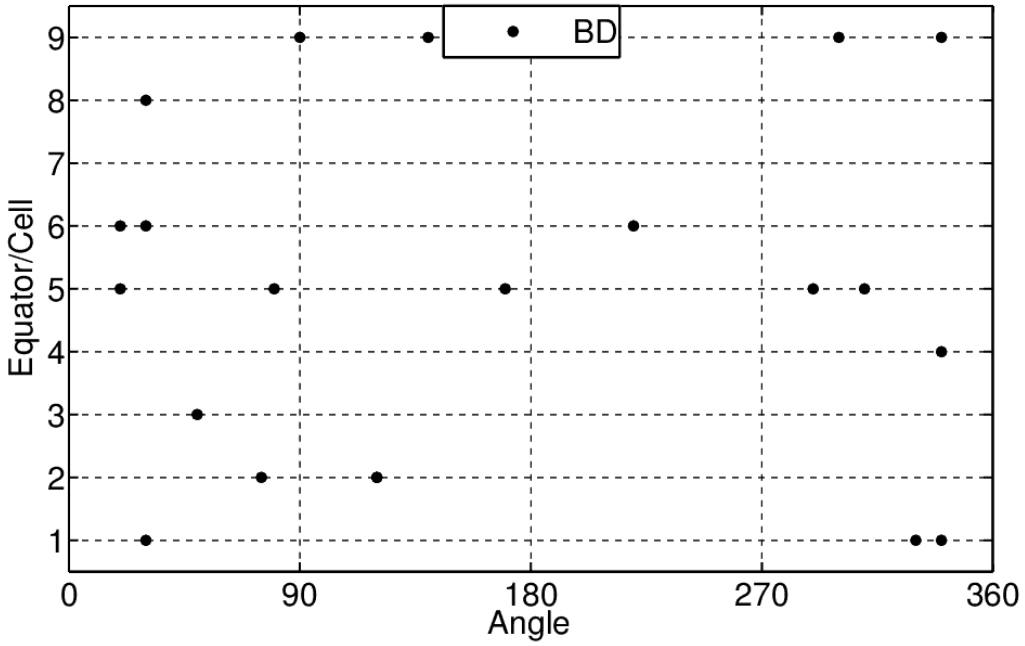

Figure 8: Distribution of quench locations found by rotating temperature mapping from June 2007 to March 2010. The angular clustering observed with second sound is also found in this diagram.

4.1.3 Inserts and vertical cryostats

Another possibility identified to be the reason for the angular accumulation is in the vertical cryostats. As the refill of the cryostats with liquid helium with $T > 2\,\mathrm{K}$ is usually done continuously, the filling lines at top and bottom of the cryostat may lead to slightly higher temperatures in the helium bath. The helium refill can be excluded, as the superfluid helium has a good thermal conductivity, the bath remains at $T = 2\,\mathrm{K}$ because the heat is distributed fast and the cryostat is pumped continuously.
Both cryostats were checked for the helium inlets, and as the angular distribution of the filling lines is symmetric and the orientation of the inserts is always the same, only the lower filling line is in the section $> 270°$, but the location is about half a meter below the first cell of the cavity and hence can be excluded.

4.1.4 Cryostat inserts

All material close to the cavity in the vertical test has to be non-magnetisable to avoid freeze-out of magnetic flux in the niobium, resulting in lower quality factors and thus higher surface resistance (e.g. [9]). If a magnetic field is applied locally, it may result in earlier thermal breakdown in this area because the generation of heat as the surface magnetic field increases.
Insert 1 at the DESY cryogenic test stand includes a waveguide all along and close to

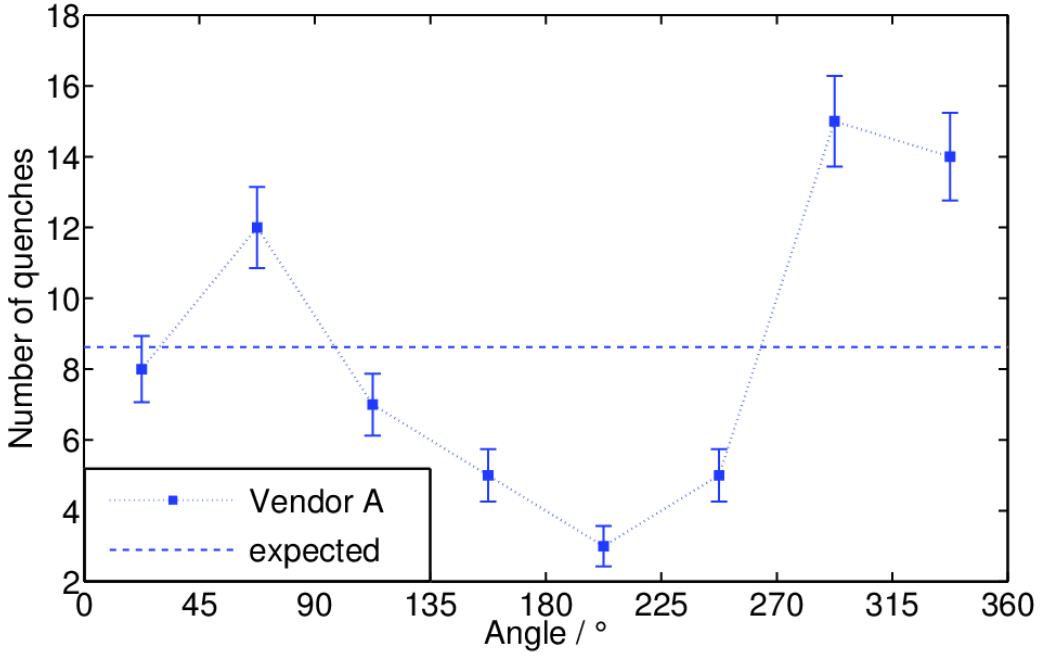

(a) Vendor A

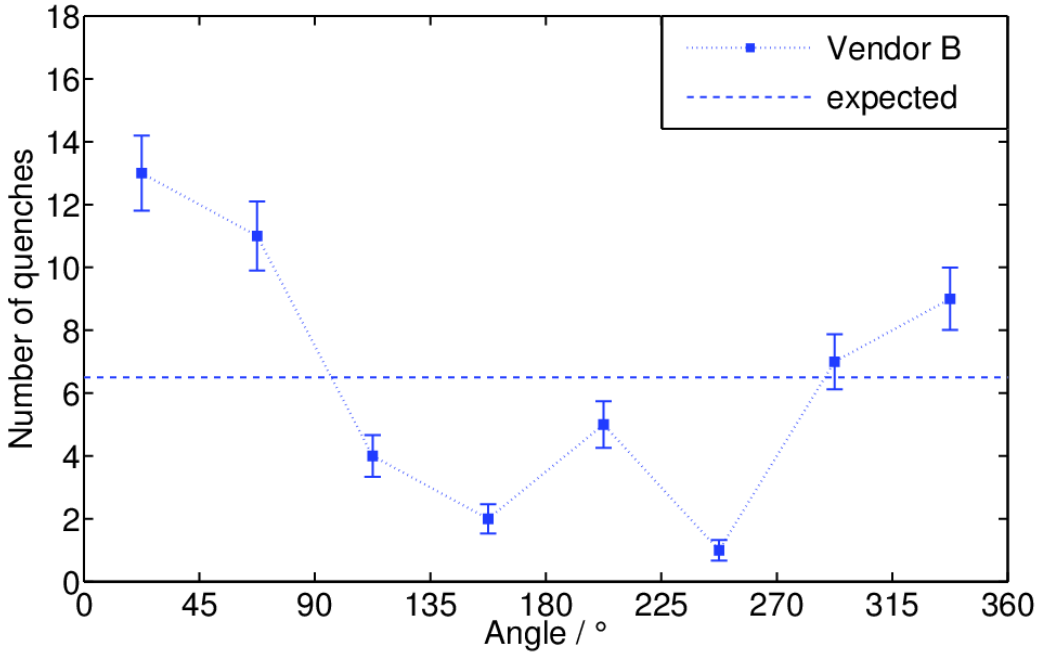

(b) Vendor B

Figure 9: Angular distribution of quench locations for each vendor.

the cavity right in the suspicious angular area. This waveguide has been tested for permeability. The measurement at several locations on the waveguide showed a relative permeability of $\mu < 1.01$, so it can be excluded as a source for a magnetic field.
Magnetic field gradient measurements with a fluxgate magnetometer showed a small magnetic field at the surface of a fixture part (so-called *horseshoe*) for the cavity in the vertical inserts of some μT in the preparation area. This part is about 20 cm away from cell 1 of the cavity. The magnetomer has been positioned close to the equator of the cell, and the fully equipped insert was placed in the cryostat to shield the earth magnetic field. The field components of the magnetic field measured at $\Phi = 315°, 45°$ at equator 1 were measured horizontally and vertically and did not not exceed $H = 0.04\,\mu$T. So a rough estimation for the absolute value of the magnetic field exposure at cell 1 of $H_{est.} = 0.1\,\mu$T is feasible and can be neglected, as it contributes only $R_s(H) \approx 0.12\,\mathrm{n\Omega}$ [10] to the overall surface resistance and heat loss.

5 Summary

In 31 cavity tests 189 quenches occured in total, resulting in 121 different quench locations, including quenches with field emission. At a first glance, two different features were found: an accumulation of quench locations in cells 1 and 2, which are the bottom cells in vertical tests. Second, about two thirds of the quench locations are located in the angular range between 270° and 90°. Most of the found quenches were, as expected, in the high surface magnetic field region of the cavity.
While the excess of quenches in cell 1 can be traced largely to one of the cavity vendors, for the accumulation in cell 2 and the angular distribution no further differentiating indicator could be found. While a number of obvious possible sources could be excluded a real explanation is still lacking.

Acknowledgement

This work is supported by the Commission of the European Communities under the 7th Framework Programme "Construction of New Infrastructures - Preparatory Phase", contract number 206711.
Special thanks to all people involved in cavity preparation and testing at 'Halle 3' at DESY.

References

[1] S. Aderhold. Optical Inspection of SRF Cavities at DESY. In *Proceedings of the 2010 International Particle Accelerator Conference (IPAC 2010)*, 2010.

[2] F. Schlander, S. Aderhold, D. Reschke, and K. Twarowski. Recent Results from Second Sound, T-Mapping and Optical Inspection of 1.3 GHz Cavities at DESY.

In *Proceedings of the 15th International Conference on RF Superconductivity*, 2011.

[3] F. Schlander, S. Aderhold, E. Elsen, D. Reschke, and M. Wenskat. Quality Assessment for Industrially Produced High-Gradient Superconducting Cavities. In *Proceedings of the 2011 International Particle Accelerator Conference (IPAC 2011)*, 2011.

[4] F. Schlander, E. Elsen, and D. Reschke. Second Sound as an Automated Quench Localisation Tool at DESY. In *Proceedings of the 15th International Conference on RF Superconductivity*, 2011.

[5] S. Aderhold, E. Elsen, F. Schlander, and L. Steder. A Common Cavity Coordinate System. Technical report, ILC HiGrade, 2011.

[6] B. van der Horst, M. Schalwat, N. Steinhau-Kuehl, and A. Matheisen. private communication.

[7] L. Lilje, C. Antoine, C. Benvenuti, D. Bloess, J. P. Charrier, E. Chiaveri, L. Ferreira, R. Losito, A. Matheisen, H. Preis, D. Proch, D. Reschke, H. Safa, P. Schmueser, D. Trines, B. Visentin, and H. Wenniger. Improved surface treatment of the superconducting TESLA cavities. *Nuclear Instruments and Methods in Physics Research A*, 526:213–227, 2004.

[8] D. Reschke. Analysis of quenches using temperature mapping in 1.3 GHz SCRF cavities at DESY. In *Proceedings of the XXIV Linear Accelerator Conference*, 2008.

[9] H. Padamsee, J. Knobloch, and T. Hays. *RF Superconductivity for Accelerators*. Wiley-VCH Verlag, Weinheim, 2008.

[10] B. Piosczyk, P. Kneisel, J. Stoltz, and J. Halbritter. Investigations of Additional Losses in Superconducting Niobium Cavities due to Frozen-In Flux. In *Proceedings of the Particle Accelerator Conference PAC1973*, 1973.